Non-Gaussian features of chaotic Hamiltonian transport‡

Roberto Venegeroles and Alberto Saa§

Centro de Matemática, Computação e Cognição, Universidade Federal do ABC, 09210-170, Santo André, SP, Brazil

E-mail: `roberto.venegeroles@ufabc.edu.br`, `asaa@ime.unicamp.br`

Abstract. Some non-Gaussian aspects of chaotic transport are investigated for a general class of two-dimensional area-preserving maps. Kurtosis, in particular, is calculated from the diffusion and the Burnett coefficients, which are obtained analytically. A characteristic time scale delimiting the onset of the Markovian regime for the master equation is established. Some explicit examples are discussed.

PACS numbers: 05.45.Ac, 05.60.Cd, 05.20.-y

‡ This work is dedicated to the memory of Prof. Radu Balescu.

§ On leave of absence from UNICAMP, Campinas, SP, Brazil.

1. Introduction

Discrete-time systems have a prominent role in many branches of nonlinear sciences. Hamiltonian (or area-preserving) maps, for instance, are particularly relevant for the modeling of classical dynamical systems[1, 2]. The study of chaos in such systems has followed two main lines. The first one considers some individual trajectories in order to explore and characterize the system main topological properties[1, 2]. The second one investigates the distribution functions of statistical ensembles or, more specifically, some transport properties of the associated maps[3]. The present work belongs to this latter group.

In the past, many investigations of transport properties for Hamiltonian maps have been motivated by the paradigmatic Chirikov-Taylor standard map[4]. Although considerable progress in the study of diffusion has been achieved in the last 25 years [5, 6, 7, 8, 9, 10, 11, 12], higher order transport coefficients have been particularly overlooked. The the fourth order coefficient B known as the Burnett coefficient[3], for instance, plays a central role in the large deviations theory: its magnitude gives the first indication of the deviation of a density function from a Gaussian packet.

Here, we consider some non-Gaussian features of the chaotic transport for Hamiltonian maps by means of high order corrections to the spectral properties of the associate Perron-Frobenius operator U. Exponential relaxation for U was rigorously established for hyperbolic systems by Pollicott and Ruelle [13, 14]. The relaxation rates γ_m, known as Pollicott-Ruelle resonances, are related to the poles $z_m = e^{\gamma_m}$ of the resolvent $R(z) = (z - U)^{-1}$. These resonances are located inside the unit circle in the complex z plane, despite that the spectrum of U is confined to the unit circle because of unitarity[15]. The normal late time evolution of density or correlations functions are dominated by the leading Pollicott Ruelle resonances (LPR). Recently, this mathematically well-established results has been confirmed in the high stochasticity approximation for some mixed systems[16, 17]. In [17], the LPR resonances are analytically calculated for the generic radial twist map[1]

$$\begin{aligned} I_{n+1} &= I_n + K\, f(\theta_n)\,, \\ \theta_{n+1} &= \theta_n + c\,\alpha(I_{n+1}) \qquad \bmod 2\pi, \end{aligned} \tag{1}$$

defined on the cylinder $-\pi \le \theta < \pi$, $-\infty < I < \infty$. We call $f(\theta)$ and $\alpha(I) = \alpha(I + 2\pi r)$, respectively, the impulse function and the rotation number. The constants c, r, and K are assumed to be real, and K is named the stochasticity parameter. One can also consider non-periodic cases by taking the limit $r \to \infty$. The LPR resonances for (1) were obtained in [17] without any high stochasticity approximation, up to corrections of second order in the wavenumber. It is shown, in particular, that the wavenumber dependence of the LPR resonances determines the transport coefficients.

In the present paper, we extend the results of [17] to higher order wavenumber corrections with the purpose of evaluating the Burnett coefficient for the map (1). Kurtosis, in particular, is then explicitly calculated. Our results are compared with numerical simulations for some specific models, namely the standard map, the sawtooth

map, and two maps with non-linear rotation numbers: a periodic one (the tangent map), and a non-periodic one (the cubic map). In all cases, a very good agreement is obtained. Our results allow us also to infer a characteristic time scale delimiting the onset of the Markovian regime for the density function. We show that such a characteristic time scale is sharper than the others previously obtained in the literature.

2. Statistical Analysis

The statistical analysis of the map (1) is best carried out in Fourier space. The conditional probability that an initial state (I_0, θ_0) evolves to a final state (I_n, θ_n) is given by $\int dI d\theta \, \rho_n(I, \theta)$. The Fourier expansion of the distribution function $\rho_n(I, \theta)$ can be written as

$$\rho_n(I, \theta) = \sum_m \int dq \, e^{i(m\theta + qI)} a_n(m, q) \,, \tag{2}$$

where the initial density is given by $\rho_0 = \delta(I - I_0)\delta(\theta - \theta_0)$, and thus $a_0(m, q) = (2\pi)^{-2} e^{-i(m\theta_0 + qI_0)}$. The expected values of the moments I^p can be calculated from the Fourier amplitudes $a_n(m, q)$ by

$$\langle I^p \rangle_n = (2\pi)^2 \left[(i\,\partial_q)^p \, a_n(q)\right]_{q=0}, \tag{3}$$

where $a_n(q) \equiv a_n(0, q)$. An alternative way to calculate the moments is given by the following expression

$$F_n(q) \equiv \langle \exp[-iq(I - I_0)] \rangle_n \,, \tag{4}$$

known as the Van Hove incoherent intermediate scattering function [3]. In the limit $q \to 0$, $F_n(q)$ becomes the generating function of the generalized moments:

$$F_n(q) = \exp \sum_{l=1}^{\infty} \frac{(-iq)^l}{l!} C_l(n), \tag{5}$$

where C_l denotes the cumulant moments[18, 19]. Defining $\Delta I \equiv I - I_0$, the first cumulants are given by

$$C_1 = \langle \Delta I \rangle_n \,, \tag{6}$$

$$C_2 = \left\langle (\Delta I)^2 \right\rangle_n - C_1^2, \tag{7}$$

$$C_3 = \left\langle (\Delta I)^3 \right\rangle_n - 3C_1C_2 - C_1^3, \tag{8}$$

$$C_4 = \left\langle (\Delta I)^4 \right\rangle_n - 3C_2^2 - 4C_1C_3 - 6C_1^2C_2 - C_1^4. \tag{9}$$

The existence of cumulant moments satisfying the equation (5) is not assumed a priori. Note, however, that $F_n(q)$ is analytic around the origin $q = 0$ if and only if all moments $\left\langle (\Delta I)^l \right\rangle_n$ exist and are finite. This condition breaks down in cases of distributions with "fat tails", like the non-Gaussian Levy stable distributions[20]. The Van Hove function (4) can be calculated explicitly from the density (2)

$$F_n(q) = \int dI d\theta \, e^{-iq(I - I_0)} \rho_n(I, \theta) = (2\pi)^2 e^{iqI_0} a_n(q). \tag{10}$$

Assuming that the evolution law for the relevant Fourier amplitude $a_n(q)$ is exponential for long times,

$$a_n(q) = \exp[n\gamma(q)]a_0(q), \tag{11}$$

and that the initial relevant amplitude is given by $a_0(q) = (2\pi)^{-2}\, e^{-iqI_0}$, the dispersion rate $\gamma(q)$ can be obtained from the limit $n \to \infty$ of the the Van Hove function

$$\gamma(q) = \lim_{n\to\infty} \frac{1}{n} \ln[F_n(q)]. \tag{12}$$

Combining the generating function (5) with the dispersion rate (12), one can define the generalized transport coefficients $\mathcal{D}_{2l}$ by

$$\mathcal{D}_{2l} \equiv \lim_{n\to\infty} \frac{1}{n}\frac{C_{2l}(n)}{(2l!)} = \frac{(-1)^l}{(2l)!}\,\partial_q^{2l}\gamma(q)|_{q=0}. \tag{13}$$

If $C_1 = 0$, the Einstein formula for the diffusion coefficient D is obtained by setting $l = 1$,

$$D \equiv \lim_{n\to\infty} \frac{1}{2n}\left\langle(\Delta I)^2\right\rangle_n = -\frac{1}{2}\partial_q^2\gamma(q)|_{q=0}, \tag{14}$$

while the Burnett coefficient B is obtained for $l = 2$,

$$B \equiv \lim_{n\to\infty} \frac{1}{4!n}\left[\left\langle(\Delta I)^4\right\rangle_n - 3\left\langle(\Delta I)^2\right\rangle_n^2\right] = \frac{1}{4!}\partial_q^4\gamma(q)|_{q=0}. \tag{15}$$

The diffusion D and the Burnett B coefficients are the bases for our analysis on non-Gaussian features of the chaotic transport for the map (1).

2.1. Accelerator modes

Before starting our analysis, however, one should warn about the so-called accelerator modes[1], corresponding to fixed points (θ_*, I_*) of (1):

$$Kf(\theta_*) = 2\pi r L_I, \qquad c\,\alpha(I_*) = 2\pi L_\theta, \tag{16}$$

where L_θ and L_I are integers satisfying the stability condition

$$|2 + cKf'(\theta_*)\alpha'(I_*)| \leq 2. \tag{17}$$

Typically, trajectories diffuse normally, although some of them may be dragged along the accelerated modes, if they do exist. These rare events become meaningful for sufficiently high time scales, resulting in anomalous diffusion of Levy type for map parameters satisfying (17). In such a case, the diffusion coefficient behaves locally between normal dynamics and accelerator modes, for which one has $D \sim n^{\beta-1}$ for $1 < \beta < 2$ [20, 21]. In the case of the standard map, these divergences result in peaks for the value of D for $K = 2m\pi$, with decreasing amplitude as K increases[1].

3. Higher order Pollicott-Ruelle Resonances

The dispersion rate (12) for the system (1) was considered in [17] up to order $\mathcal{O}(q^2)$ by means of the decomposition of the resolvent $R(z) = (z - U)^{-1}$, based on the projection operator techniques utilized by Hasegawa and Saphir[22] and Balescu[20] for the standard map. The operator U defines the law of evolution of the Fourier amplitudes, $a_n(q) = U^n a_0(q)$. Its iteration U^n can be formally obtained through the identity $\oint_C dz R(z) z^n = 2\pi i U^n$, where the contour of integration lies outside the unit circle. One then introduces the mutually orthogonal projection operators $P = |q, 0\rangle \langle q, 0|$, which selects the relevant state, and its complement $Q = 1 - P$, leading to

$$a_n(q) = \frac{1}{2\pi i} \oint_C dz \, \frac{z^n}{z - \sum_{j=0}^{\infty} z^{-j} \Psi_j(q)} \, a_0(q), \tag{18}$$

where $\Psi_j(q)$ are the so-called memory functions for the system (1). The resulting integral is solved by the method of residues by truncating the infinite denominator series at $j = N$ and then taking the limit $N \to \infty$. The nontrivial leading pole was evaluated in the limit $n \to \infty$ by the well known Newton-Raphson iterative method starting with $z_0 = 1$ [17].

The $\mathcal{O}(q^4)$ correction of the LPR resonances can be obtained by introducing into the denominator of the equation (18) the $\mathcal{O}(q^4)$ corrections to the value of z,

$$z = 1 - Dq^2 + \mathcal{O}(q^4) \tag{19}$$

and repeating the same steps done in [17]. Taking into account that $\Psi_0(q) = 1 + \mathcal{O}(q^2)$ and $\Psi_{j\geq 1}(q) = \mathcal{O}(q^2)$, the higher order LPR resonance can be rewritten as

$$\gamma(q) = \ln \sum_{j=0}^{\infty} (1 + jDq^2) \Psi_j(q) + \mathcal{O}(q^6). \tag{20}$$

The memory functions $\Psi_j(q)$ are the same ones obtained originally in [17] for the system (1)

$$\Psi_0(q) = \mathcal{J}_0(-Kq)\,, \tag{21a}$$

$$\Psi_1(q) = \sum_m \mathcal{J}_{-m}(-Kq) \mathcal{J}_m(-Kq) \, \mathcal{G}_0(r, mc)\,, \tag{21b}$$

$$\begin{aligned} \Psi_{j\geq 2}(q) = & \sum_{\{m\}} \sum_{\{\lambda\}^\dagger} \mathcal{J}_{-m_1}(-Kq) \, \mathcal{J}_{m_j}(-Kq) \, \mathcal{G}_{\lambda_1}(r, m_1 c) \times \\ & \times \prod_{i=2}^{j} \mathcal{G}_{\lambda_i}(r, m_i c) \, \mathcal{J}_{m_{i-1} - m_i} \left[-K \left(q + r^{-1} \sum_{k=1}^{i-1} \lambda_k \right) \right]. \end{aligned} \tag{21c}$$

The Fourier decompositions of the $\alpha(I)$ and $f(\theta)$ functions are, respectively,

$$\mathcal{G}_l(r, x) = \frac{1}{2\pi} \int d\theta \, \exp\{-i[x\alpha(r\theta) - l\theta]\}\,, \tag{22}$$

$$\mathcal{J}_m(x) = \frac{1}{2\pi} \int d\theta \, \exp\{-i[m\theta - xf(\theta)]\}\,. \tag{23}$$

Hereafter, the following convention is adopted: wavenumbers denoted by Roman indices can only take non-zero integer values, whereas wavenumbers denoted by Greek indices can take all integer values, including zero. For fixed j, the sets of wavenumbers are defined by $\{m\} = \{m_1, \ldots, m_j\}$ and $\{\lambda\}^\dagger = \{\lambda_1, \ldots, \lambda_j\}$, where the dagger denotes the restriction $\sum_{i=1}^{j} \lambda_i = 0$. We introduce also the following series expansion for the function (23)

$$\mathcal{J}_m(x) = \delta_{m,0} + \sum_{n=1}^{\infty} c_{m,n}\, x^n, \tag{24}$$

where

$$c_{m,n} = \frac{1}{2\pi}\frac{i^n}{n!}\int d\theta\, f^n(\theta)\, e^{-im\theta}. \tag{25}$$

4. Transport Coefficients and Kurtosis

The general exact diffusion coefficient can be obtained by using the definition (14) and the LPR resonance (20), taking into account (21a)-(21c),

$$\frac{D}{D_{ql}} = 1 + 2\sum_{m\geq 1} \sigma_{m,m}\,\mathrm{Re}[\mathcal{G}_0(r, mc)] + \sum_{j=2}^{\infty}\sum_{\{m\}}\sum_{\{\lambda\}^\dagger} \sigma_{m_1,m_j}\,\mathcal{G}_{\lambda_1}(r, m_1 c)\times$$
$$\times \prod_{i=2}^{j} \mathcal{G}_{\lambda_i}(r, m_i c)\,\mathcal{J}_{m_{i-1}-m_i}\left(-\frac{K}{r}\sum_{k=1}^{i-1}\lambda_k\right), \tag{26}$$

where the condition $c_{0,1} = 0$ (and thus $C_1 = 0$) is requeried, $D_{ql} = -c_{0,2}\, K^2$ is the quasilinear diffusion coefficient and $\sigma_{m,m'} = c_{-m,1} c_{m',1}/c_{0,2}$ [17]. The diffusion coefficient (26) gives the lowest order macroscopic description of the diffusion process. If the evolution process is asymptotically truly diffusive, then the angle-averaged density should have a Gaussian contour after a sufficiently long time. A first indication of the deviation of a density function from a Gaussian packet is given by the Burnett coefficient B defined by (15). The dimensionless fourth order cumulant

$$\kappa(n) \equiv \frac{\langle(\Delta I)^4\rangle_n}{\langle(\Delta I)^2\rangle_n^2} \tag{27}$$

is usually called the kurtosis. For Gaussian densities, $B = 0$ and $\kappa = 3$ for all times. Combining (14), (15), and (27), we obtain for sufficiently long times

$$\kappa = 3 + \frac{6B/D^2}{n}. \tag{28}$$

The Burnett coefficient B can be evaluated in the chaotic regime by truncating of the resonance (20) at $j = 2$ so that (15) can now be applied to (20), yielding

$$B \approx -\frac{5}{2}D^2 + 2DD_{ql} - \frac{1}{2}D\,\partial_q^2\Psi_1 + \frac{1}{4!}\partial_q^4(\Psi_0 + \Psi_1 + \Psi_2) \tag{29}$$

calculated at $q = 0$. In order to verify these results, we calculate the Burnett coefficients and its respective kurtosis for some particular cases of maps (1) and compare with the respective numerical simulations. To this purpose, it is important to choose intermediate values of n, since exaggerated values tends to wash non-Gaussian fluctuations away quickly.

4.1. The standard map

The standard map corresponds to the choice $c\alpha(I) = I$ and $f(\theta) = \sin\theta$ in (1). The memory functions (21a)-(21c) are rather simple for the case of linear rotation number since one has $\mathcal{G}_\lambda(1, x) = \delta_{\lambda,x}$. For the standard map, $\mathcal{J}_m(x)$ is the Bessel function of the first kind $J_m(x)$, $D_{ql} = K^2/4$ and $\sigma_{m,m'} = (\pm\delta_{m,\pm1})(\pm\delta_{m',\pm1})$. The final expressions for D and B in the chaotic regime for the standard map are given by

$$\frac{D}{D_{ql}} = 1 - 2J_2(K) + \mathcal{O}(K^{-1}), \tag{30}$$

$$\frac{B}{D_{ql}^2} = -\frac{1}{4} + J_0(K) + 2J_2(K) + J_4(K) + \frac{1}{2}J_4(2K) + \mathcal{O}(K^{-1}). \tag{31}$$

The kurtosis (28) can be evaluated straightforwardly. Fig. 1 depicts the calculated

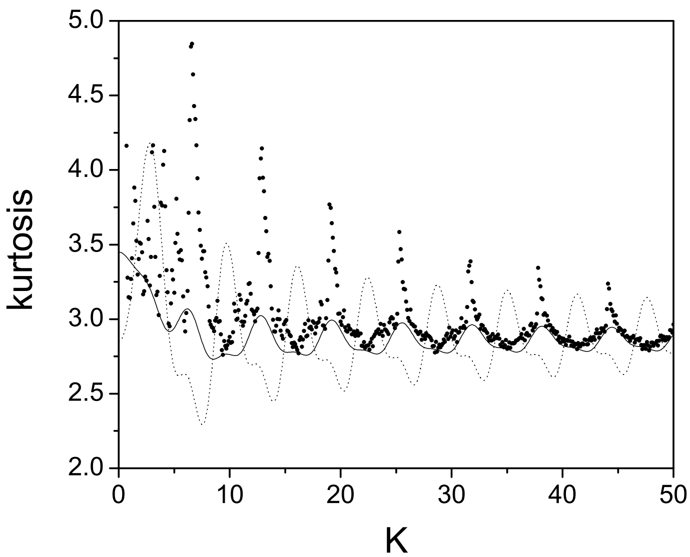

Figure 1. Kurtosis as a function of K for the standard map for $c = 1$ and $n = 10$. The dots correspond to numerically computed values and the solid line to the theoretical result in the chaotic regime, up to terms of order $\mathcal{O}(K^{-1})$. For each value of K, 10^5 random initial conditions are considered in the numerical simulation. This plot shows good agreement with numerical calculations although the accelerator modes give rise to spikes in the figure. The dashed line corresponds to the Kurtosis calculated from the results of Tabet *et. al* presented in [24]. See Section 4.5 for further details. As one can see, the present results give rise to a superior description.

kurtosis and the results of numerical simulations for the standard map. We notice, in particular, the presence of accelerator modes.

4.2. The sawtooth map

The sawtooth map corresponds to $c\alpha(I) = I$ and $f(\theta) = \theta$. As for the standard map, $\mathcal{G}_\lambda(1, x) = \delta_{\lambda,x}$. On the other hand, in this case, $\mathcal{J}_m(x) = \frac{\sin[\pi(m-x)]}{\pi(m-x)}$, $D_{ql} = K^2\pi^2/6$, and $\sigma_{m,m'} = \frac{6}{\pi^2}\frac{(-1)^{m-m'}}{mm'}$, leading to

$$\frac{D}{D_{ql}} = 1 - \frac{1}{6}S_3(K), \tag{32}$$

$$\frac{B}{D_{ql}^2} = -\frac{1}{5} - \frac{1}{3}S_3(K) + \frac{3+2K}{2+K}C_4(K) + \frac{9+10K+3K^2}{(2+K)^2}S_5(K), \tag{33}$$

both up to $\mathcal{O}(K^{-2})$ order, where the function $S_j(K)$ and $C_j(K)$ are given by

$$S_{2j+1}(K) \equiv \sum_{m=1}^{\infty} \frac{72\sin(\pi m K)}{(K+2)(\pi m)^{2j+1}}\,, \tag{34}$$

$$C_{2j}(K) \equiv \sum_{m=1}^{\infty} \frac{72\cos(\pi m K)}{(K+2)(\pi m)^{2j}}\,, \tag{35}$$

and $S_{2j}(K) = C_{2j+1}(K) = 0$. Fig. 2 presents the comparison of the kurtosis calculated from (32) and (33) with the numerical simulations for the sawtooth map. As one can

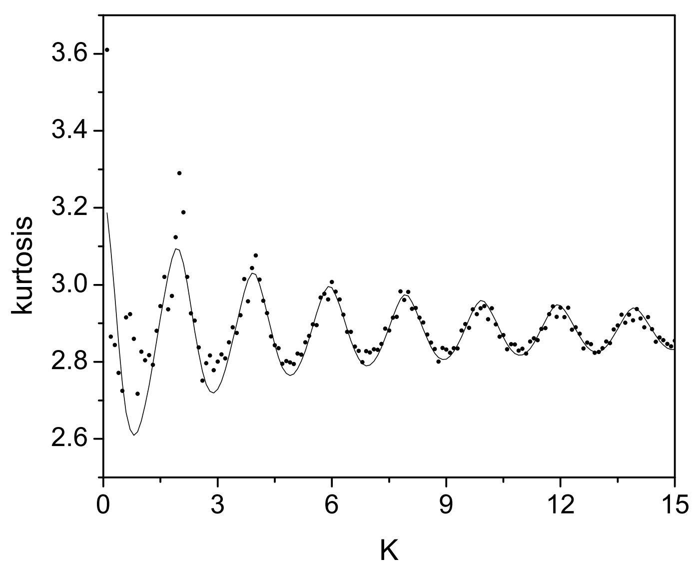

Figure 2. Kurtosis as a function of K for the sawtooth map for $c = 1$ and $n = 10$. For each value of K, 10^5 random initial conditions are considered in the numerical simulation. This plot shows excellent agreement between the theory and the numerical simulations.

see, the absence of accelerator modes contributes with the excellent agreement of the numerical simulation with the theoretical predictions.

A pertinent comment here is that, as one can see from Figures 1 and 2, for a fixed n, the limit for the kurtosis κ is not 3 as $K \to \infty$. From the asymptotic values of (30)-(31)

and (32)-(33), it is easy to show that, for $n = 10$, the kurtosis in the limit $K \to \infty$ tend to the values 57/20 and 72/25, respectively, for the standard and sawtooth maps. Similar results hold also for other maps. The conclusion that, for fixed n, the limit of high stochasticity is not enough to assure a Gaussian regime is interesting and certainly would deserve a deeper analysis.

4.3. The tangent map

We call the tangent map the choice of $f(\theta) = \theta$ and $\alpha(I) = \tan(I/2)$ in (1). It is our first example of a map with a non-linear rotation number. The functions $\mathcal{J}_m(x)$ are the same ones from the sawtooth map. The functions $\mathcal{G}_\ell(1, x)$ can be calculated by complex residues from their definition (22). Introducing the variable $s = \tan(\theta/2)$ and taking into account the identity $i \arctan s = \operatorname{arctanh} is$, we have

$$\mathcal{G}_\ell(1, x) = \frac{1}{\pi} \int_{-\infty}^{\infty} \frac{(1 - is)^{\ell-1} e^{ixs}}{(1 + is)^{\ell+1}} ds. \tag{36}$$

For $\ell = 0$, (36) has two single poles on the complex plane located at $z = \pm i$. For positive x and negative x, one closes the integration path of (36), respectively, by the positive $\Im(z)$ and negative $\Im(z)$ semiplanes, giving simply

$$\mathcal{G}_0(1, x) = e^{-|x|}. \tag{37}$$

Let us consider now $\ell > 0$. Notice that $\mathcal{G}_\ell(1, x)$ can be evaluated for negative ℓ by observing that $\mathcal{G}_{-\ell}(1, x) = \mathcal{G}_\ell(1, -x)$. The integral (36) has a unique pole of order $\ell + 1$ at $z = i$ for $\ell > 0$. In such a case, for negative x we can close the integration path in the negative $\Im(z)$ semiplane and conclude that $\mathcal{G}_\ell(1, x) = 0$ for $\ell > 0$ and $x < 0$. For positive x we close the integration path in the positive $\Im(z)$ semiplane and obtain

$$\mathcal{G}_l(1, x) = 2 \frac{(-1)^\ell}{\ell!} \left[\frac{d^\ell}{ds^\ell} \left((s + 1)^{\ell-1} e^{-xs} \right) \right]_{s=1}, \tag{38}$$

for $\ell > 0$ and $x \geq 0$. As illustrative examples, the very first functions (38) are given by

$$\mathcal{G}_1(1, x) = 2xe^{-x}, \tag{39}$$

$$\mathcal{G}_2(1, x) = 2x(x - 1)e^{-x}, \tag{40}$$

$$\mathcal{G}_3(1, x) = \frac{2}{3} x(2x^2 - 6x + 3)e^{-x}, \tag{41}$$

for $x \geq 0$.

The expressions for D and B are obtained from (26) and (29), respectively. Fig. 3 depicts the comparison between the calculated diffusion and kurtosis for the tangent map and the numerical simulations.

4.4. The cubic map

We call the cubic map the choice $\alpha(I) = I^3/3$ and $f(\theta) = \sin \theta$ in (1). It is our example of map with non-periodic non-linear rotation number. Due to the non-periodicity, some

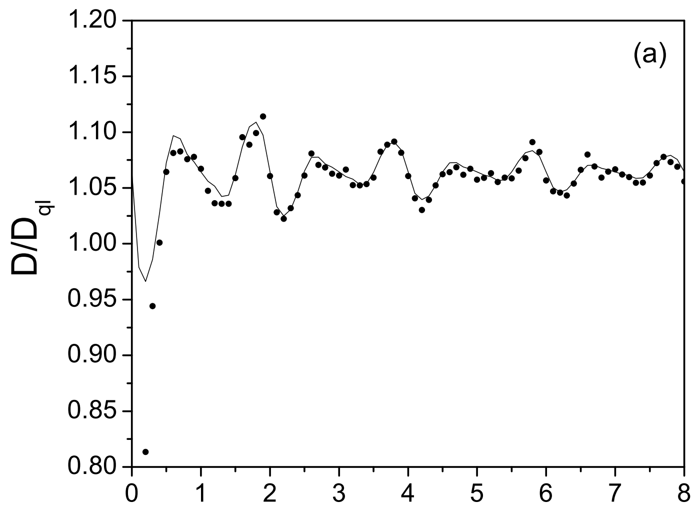

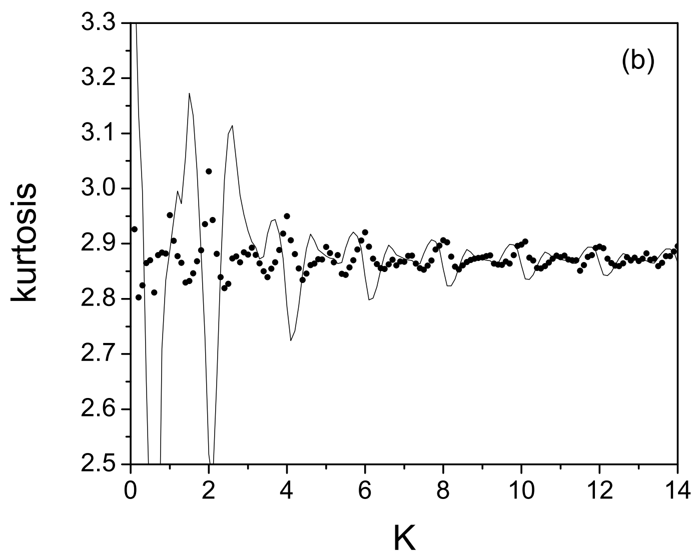

Figure 3. Diffusion (a) and Kurtosis (b) as a function of K for the tangent map with $c = 3$ and $n = 10$. The dots corresponds to the numerically computed values and the solid line to the theoretical result in the chaotic regime. For each value of K, 10^5 random initial conditions are considered in the numerical simulations. Both plots also exhibit good agreement between the predictions and the numerical simulations.

parts of our formalism shall be modified. First, we rewrite the function (22) in the following way

$$\mathcal{G}_\lambda(r,x) = \frac{1}{2\pi r}\int_{-\pi r}^{\pi r} du\, e^{-i(x\alpha(u)-\lambda r^{-1}u)}. \qquad (42)$$

The non-periodic rotation number corresponds to the limit $r \to \infty$. In this case, we apply the following overall replacements in our formulas

$$r^{-1}\lambda \longrightarrow s, \tag{43}$$

$$r^{-j} \sum_{\{\lambda_1,\ldots,\lambda_j\}} \longrightarrow \int ds_1 \times \ldots \times ds_j \,, \tag{44}$$

$$r\, \mathcal{G}_\lambda(r,x) \longrightarrow \mathcal{G}(s,x), \tag{45}$$

where the function $\mathcal{G}(s,x)$ is now given by

$$\mathcal{G}(s,x) = \frac{1}{2\pi}\int dI\, e^{-i(x\alpha(I)-sI)}. \tag{46}$$

Performing analogous calculations to the periodic case, we obtain the new set of memory functions

$$\Psi_0(q) = \mathcal{J}_0(-Kq)\,, \tag{47a}$$

$$\Psi_1(q) = \sum_m \mathcal{J}_{-m}(-Kq)\mathcal{J}_m(-Kq)\,\mathcal{G}(0,mc)\,, \tag{47b}$$

$$\Psi_{j\geq 2}(q) = \sum_{\{m\}} \mathcal{J}_{-m_1}(-Kq)\,\mathcal{J}_{m_j}(-Kq) \int_{\mathcal{S}^\dagger} d\vec{s}\,\mathcal{G}(s_1,m_1c)\times$$
$$\times \prod_{i=2}^{j} \mathcal{G}(s_i,m_ic)\,\mathcal{J}_{m_{i-1}-m_i}\left[-K\left(q+\sum_{k=1}^{i-1}s_k\right)\right], \tag{47c}$$

where $d\vec{s} = ds_1 \times \ldots \times ds_j$, with the domain of integration defined by $S^\dagger = \left\{(s_1,\ldots,s_j) : \sum_{i=1}^{j} s_i = 0\right\}$. Finally, the diffusion coefficient will be given by

$$\frac{D}{D_{ql}} = 1 + 2\sum_{m=1}^{\infty}\sigma_{m,m}\,\mathrm{Re}[\mathcal{G}(0,mc)] + \sum_{j=2}^{\infty}\sum_{\{m\}}\sigma_{m_1,m_j}\int_{\mathcal{S}^\dagger} d\vec{s}\,\mathcal{G}(s_1,m_1c)\times$$
$$\times \prod_{i=2}^{j}\mathcal{G}(s_i,m_ic)\,\mathcal{J}_{m_{i-1}-m_i}\left(-K\sum_{k=1}^{i-1}s_k\right). \tag{48}$$

Note that, for non-periodic linear rotation numbers, we have $\mathcal{G}(s,x) = \delta(s-x)$, and the diffusion formula (48) coincides with the periodic linear rotation number version of (26).

For the cubic map, the function $\mathcal{G}(s,x)$ can be calculated by means of Airy functions[23]

$$\mathcal{G}(s,x) = x^{-1/3}\mathrm{Airy}(-x^{-1/3}\,s). \tag{49}$$

The power dependence $x^{-1/3}$ in (49) may create a false impression of divergence of the series (48) for the cases where $c^{1/3} \ll 1$. In order to avoid this problem, one can define

$$c \equiv c_1c_2, \qquad c_2^{1/3}I \equiv x, \tag{50}$$

and rewrite the cubic map as

$$\begin{aligned} x_{n+1} &= x_n + Kc_2^{1/3}\mathrm{sen}\,\theta_n\,,\\ \theta_{n+1} &= \theta_n + c_1\,x_{n+1}^3/3 \qquad \mathrm{mod}\,2\pi. \end{aligned} \tag{51}$$

From (50), it follows that $(\Delta x)^2 = c_2^{2/3}(\Delta I)^2$ and $D_{ql}^{(x)} = c_2^{2/3} D_{ql}^{(I)}$. Hence, the rate D/D_{ql} for the cubic map is invariant under the rescaling

$$\frac{D}{D_{ql}}(c, K) \equiv \frac{D}{D_{ql}}(c_1 c_2, K) = \frac{D}{D_{ql}}(c_1, K c_2^{1/3}). \tag{52}$$

Assuming that

$$K \gg c^{-1/3}, \tag{53}$$

the rescaling

$$c_1 = K^3 c, \qquad c_2 = K^{-3} \tag{54}$$

prevents any potential problem of divergence for maps with small c.

For small values of K, the memory functions $\Psi_{j\geq 2}(q)$ give rise to high oscillatory combinations of Airy and Bessel functions, with integrals that are very difficult to estimate. On the other hand, the high stochastic condition (53) implies that $\mathrm{Airy}(c_1^{-1/3}s) \approx \mathrm{Airy}(0)$ even for sufficiently high values of $|s|$ for which Bessel functions already decay as $J_m(s) \sim e^{is}|s|^{-1/2}$. Thus, in this regime, the rate D/D_{ql} for the cubic map can be estimated by

$$\left|\frac{D}{D_{ql}} - 1\right| \leq \sum_{j=1}^{\infty} \frac{b_j}{(K c^{1/3})^j}, \tag{55}$$

where

$$\begin{aligned} b_1 &= 2\mathrm{Airy}(0), &(56)\\ b_{j\geq 2} &= \mathrm{Airy}^j(0) \sum_{\{m\}} \frac{(\pm\delta_{m_1,\pm 1})(\pm\delta_{m_j,\pm 1})}{(m_1 \times \ldots \times m_j)^{1/3}} \times \\ &\quad \times \int ds_1 \times \ldots \times ds_{j-1} \prod_{i=2}^{j} J_{m_{i-1}-m_i}\left(-\sum_{k=1}^{i-1} s_k\right) \\ &= \frac{1}{2}[2\mathrm{Airy}(0)]^j \sum_{\{m_i = 2l_i+1\}} \frac{(\pm\delta_{m_1,\pm 1})(\pm\delta_{m_j,\pm 1})}{(m_1 \times \ldots \times m_j)^{1/3}} = 8\mathrm{Airy}^2(0)\,\delta_{j,2}, &(57) \end{aligned}$$

leading, as expected, to $\lim_{K\to\infty} D = D_{ql}$. Indeed, the quasilinear regime for the diffusion is rapidly attained for high values of K, without oscillations, see Fig. 4. Similar results hold for any rotation number of the type $\alpha(I) \propto I^p$, for $p > 1$. In such cases, $\mathcal{G}(x, 0) \propto x^{-1/p}$ and (53) shall be replaced by $K \gg c^{-1/p}$.

Regarding the kurtosis for the cubic map, similar arguments can be used to show that

$$\kappa \sim 3 - \frac{6}{5n}, \tag{58}$$

also without oscillations for $K \gg c^{-1/3}$. Since the diffusion is quasiliner for such values of K, the memory functions Ψ_j can be disregarded for all $j \geq 1$. In this limit, from (29), we have simply $B/D^2 \sim -1/5$, and, hence, leading to (58). Fig. 5 depicts the behavior of the kurtosis for the cubic map.

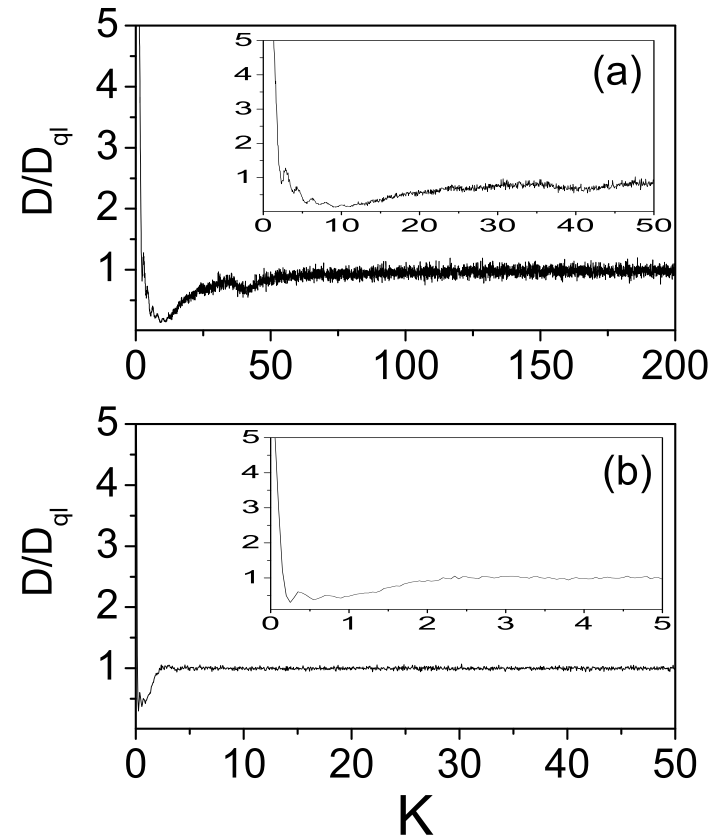

Figure 4. Numerically calculated diffusion for the cubic map with $c = 10^{-4}$ (a) and $c = 10^{-1}$ (b). For each value of K, 10^5 random initial conditions are considered in the numerical simulations. According to our results (see Section 4.4), quasilinear behavior is expected to occur for $K \gg c^{-1/3}$. From the figures, quasilinear diffusion clearly takes place for $K > 21$ and $K > 2$, respectively, in accordance to our theoretical predictions.

4.5. Comparison with previous approaches

It is instructive to compare our results with others previously obtained in the literature in the context of standard map. Tabet *et al*[24], for instance, do not calculated the Burnett coefficient explicitly. They used, instead, the Fourier path technique[1, 5] to calculate the moments $\langle(\Delta I)^4\rangle_n$ and $\langle(\Delta I)^2\rangle_n$, from which we can evaluate the respective rate B/D^2 by means of the definitions (14) and (15). One has

$$\frac{B}{D^2} = -\frac{1}{4} + 3J_2(K) + 2J_4(2K) + \mathcal{O}(K^{-1}). \tag{59}$$

On the other hand, Balescu[25] utilizes a related, but somewhat different approach from ours to calculate kurtosis for the standard map. He also does not calculate explicitly the kurtosis nor the Burnett coefficient, but he present a non-Markovian approach for

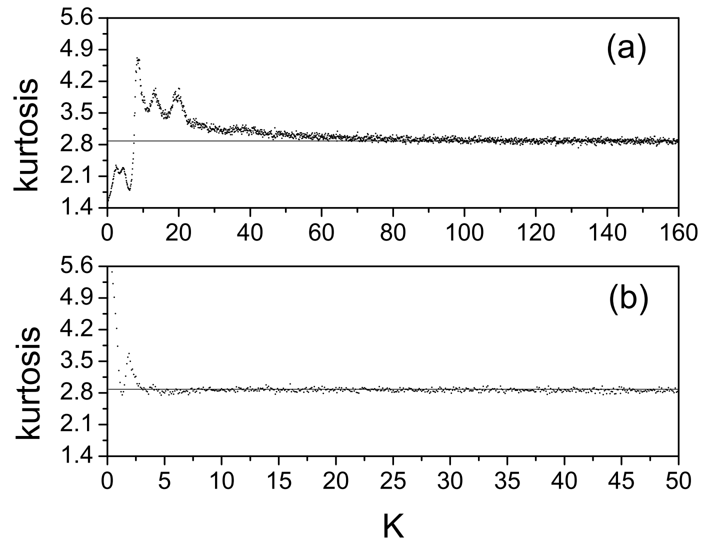

Figure 5. Numerically calculated kurtosis for the cubic map with $c = 10^{-4}$ (a) and $c = 10^{-1}$ (b). For each value of K, 10^5 random initial conditions are considered in the numerical simulations. As the diffusion coefficient (Fig. 4), quaselinear behavior is expected to occur for $K > 21$ and $K > 2$, respectively.

the relevant amplitudes, for which the propagator $F_n(q)$ is given by

$$F_n \approx \Psi_0^n + (n-2)\Psi_0^{n-3}\Psi_2 + \frac{1}{2}(n-5)(n-6)\Psi_0^{n-6}\Psi_2^2 \tag{60}$$

for $n \geq 6$, where memory functions $\Psi_{j\geq 3}$ contributing with terms of order $\mathcal{O}(K^{-1})$ are disregarded. The corresponding Burnett coefficient can be calculated by means of (12) and (15), leading exactly to the same result we have gotten here

$$\frac{B}{D^2} = -\frac{1}{4} + J_0(K) + J_2(K) + J_4(K) + \frac{1}{2}J_4(2K) + \mathcal{O}(K^{-1}), \tag{61}$$

compare with (31) and (30). Although the equations (59) and (61) have the same asymptotic value, they are enough different even in the high stochastic regime. However, it becomes difficult to note differences in the kurtosis calculated in both cases for large values of n (Tabet *et al* used $n = 50$, for instance). For relatively smaller values, the equation (61) gives a much better agreement with numerical simulations than (59), as one can see in the Fig.1.

5. Gaussian characteristic time scale

Equation (28) suggests the existence of a characteristic time: the Gaussian time scale n_G, defined by

$$n_G \equiv \max_K \left\lceil 6(|B|/D^2) \right\rceil, \tag{62}$$

where $\lceil x \rceil = \inf\{n \in Z | x \leq n\}$ is the ceiling function. For $n \gg n_G$, the transport process is typically Gaussian, up to order $\mathcal{O}(q^6)$. In fact, for $n \gg n_G$, the expansion of the propagator $\exp[n\gamma(q)]$ gives the well known Gaussian density

$$\begin{aligned} \exp[n\gamma(q)] &= 1 - Dnq^2 + \frac{1}{2}Dn^2\frac{\kappa}{3}\,q^4 + \mathcal{O}(q^6) \\ &\approx \exp(-Dnq^2) + \mathcal{O}(q^6), \end{aligned} \tag{63}$$

where κ is given by equation (28). The Gaussian time scale n_G has also a second and no lesser important interpretation: in the regime $n \gg n_G$, the time evolution of the relevant amplitudes becomes Markovian. This is easy to realize since, for $n \gg n_G$, the higher order corrections can be neglected and the LPR resonance (20), which gives the exact expression for the normal diffusion coefficient[17], can be taken as the approximate propagator. Hence, for $n \gg n_G$, equation (11) holds perfectly and, furthermore, becomes the following Markovian master equation

$$a_n(q) \approx \left(\sum_{j=0}^{\infty} \Psi_j(q)\right) a_{n-1}(q). \tag{64}$$

The Gaussian time scale n_G is sharper than some characteristic times obtained previously in the literature, as, for instance, Balescu's memory time n_M introduced in [25]. Balescu obtained the propagator (60) by means of the general non-Markovian Bandtlow and Coveney master equation[26]. The convolution of the master equation is truncated at the memory time n_M, leading to

$$a_{n+1}(q) \approx \sum_{j=0}^{n_c} \Psi_j(q)\, a_{n-j}(q), \tag{65}$$

where

$$n_c = \begin{cases} n & \text{for } n \leq n_M, \\ n_M & \text{for } n > n_M. \end{cases} \tag{66}$$

Notice that, for $n \gg n_M$, the equation (65) becomes the Markovian equation (64). By means of some numerical experiments with the decay of memory functions for the standard map, Balescu concludes that $n_M = 4$ and, in such a case, obtained equation (60).

Evidently, we expect that the two time scales to be related by $n_G = n_M + 1$. The advantage of n_G is that it can be calculated judiciously by means of (62) for a generic class of systems like (1). Moreover, typically, n_G is sharper than Balescu's memory time. In Fig. 6 we can observe the behavior of the rate $\lceil 6|B|/D^2 \rceil$ as a function of K for the standard map and for the sawtooth map. The theoretical prediction given by (62) is confirmed for $K > 4$ for the standard map ($K > 2$ for the sawtooth map). However, it is important also to point out that the Gaussian time (62) evidently fails in the description of the weak-stochasticity regime, since the effects of the KAM surfaces and the stable islands become increasingly important as K decreases, requiring not only the calculation of further memory functions but the inclusion of the source term involving initial conditions (see [26]). For instance, let us consider the equation (65) for

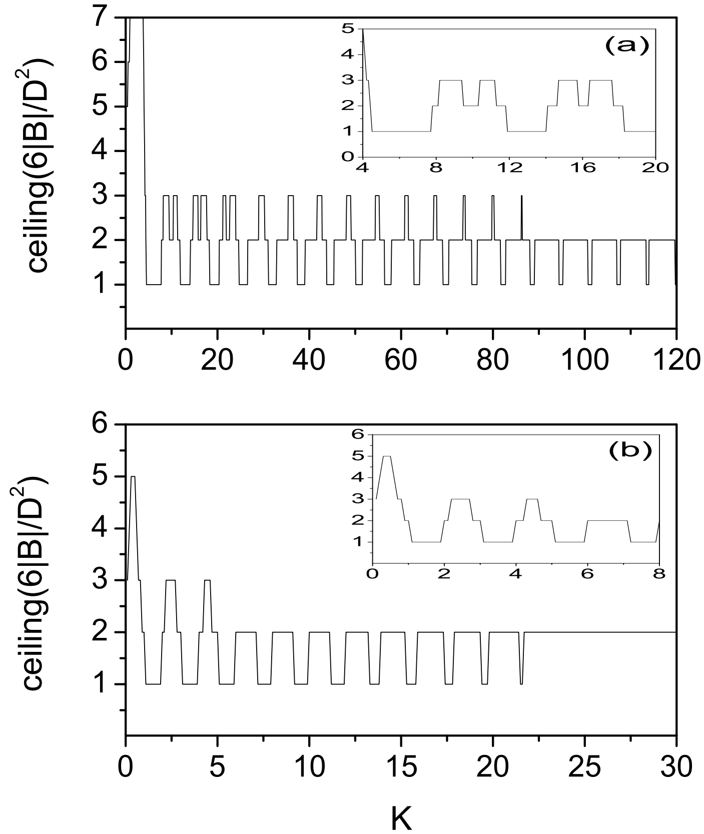

Figure 6. Gaussian time scale as a function of K for the standard map (a) and for the sawtooth map (b), both with $c = 1$ and $n = 10$. For the standard map, we have $n_G = 3$ (or $n_M = 2$) for $K > 4$ (for the sawtooth map, for $K > 2$), in excellent agreement with our expectations. For larges K, n_M falls to 1 indicating the absence of correlations of order $K^{-1/2}$ for large n, for both cases.

the general linear rotation number case by applying the Balescu approach for $n_M = 2$ (see Appendix). New calculations of the Burnett coefficient by means of the propagator (A.6) gives

$$B \approx -\frac{5}{2}D^2 + 2DD_{ql} + \frac{1}{4!}\partial_q^4(\Psi_0 + \Psi_2)_{q=0}, \tag{67}$$

that is exactly the equation (29) for $\Psi_1 = 0$! Hence, we should expect in the chaotic regime

$$n_G = 3 \qquad \text{for} \quad c\,\alpha(I) = I. \tag{68}$$

6. Summary and Discussion

In this paper, we have performed a detailed analysis of the non-Gaussian aspects of the normal transport in Hamiltonian discrete systems. The general class of area-preserving

maps represented by (1) has been chosen because it comprises a large number of physical situations and has the paradigmatic standard map as a particular case. The map (1) was recently studied in [17], where the basis for the study of the higher order transport coefficients, including nonhyperbolic systems, was initiated. The LPR resonances of the system (1) were enhanced in its wavenumber dependence with corrections of order q^4, so that the corresponding fourth order Burnett coefficient could be evaluated. Numerical simulations were performed for four particular cases of (1) and excellent agreement with the theoretical predictions is obtained.

We have established also a Gaussian time scale n_G given by equation (62). For $n \gg n_G$, the density function acquires a Gaussian countour and its time evolution is ruled by a Markovian master equation. We also show that n_G is related with the memory time n_M defined by Balescu [25] by $n_G = n_M + 1$. For maps such that $c\alpha(I) = I$ we conclude that $n_G = 3$, a sharper result than Balescu's memory time n_M.

Acknowledgments

The authors thanks E. Guéron for enlightening discussions and G. Dalpian for providing computing resources. This work was supported by funds of FAPESP, CNPq, and UFABC. A.S. is grateful to Prof. V. Mukhanov for the warm hospitality at the Ludwig-Maximilians-Universität, Munich, where part of this work was carried out.

Appendix A. Balescu's approach for $n_M = 2$

In this appendix we show that the cuttof time n_M in the Balescu equation (65) can be taken as $n_M = 2$ in the chaotic regime. For every calculation, we retain arbitrary powers of Ψ_0 and terms of order Ψ_2 and Ψ_2^2 (recalling that $\Psi_1 = 0$ for the linear rotation number case). Equation (65) in the form $a_{n+1}(q) = F_n(q)\, a_n(q)$ where

$$F_{n+1}(q) = \sum_{j=0}^{n_c} \Psi_j(q) F_{n-j}(q), \qquad F_0(q) \equiv 1, \tag{A.1}$$

with $n_c = n$ for $n \leq n_M$ and $n_c = n_M$ for $n > n_M$. The next six propagators F_n are given by

$$\begin{aligned}
F_1 &= \Psi_0, \\
F_2 &= \Psi_0^2, \\
F_3 &= \Psi_0^3 + \Psi_2, \\
F_4 &= \Psi_0^4 + 2\Psi_0\Psi_2, \\
F_5 &= \Psi_0^5 + 3\Psi_0^2\Psi_2, \\
F_6 &= \Psi_0^6 + 4\Psi_0^3\Psi_2 + \Psi_2^2.
\end{aligned}$$

Thus, we can write a general expression for F_n:

$$F_n = \Psi_0^n + x_n \Psi_0^{n-3}\Psi_2 + y_n \Psi_0^{n-4}\Psi_2^2, \tag{A.2}$$

with the following initial conditions (note that $\Psi_0^k\Psi_2^2 \sim \Psi_2^2 \sim q^4$ for finite k)

$$\begin{cases} x_1 = 0, & x_{n\geq 2} = n-2, \\ y_{n\leq 5} = 0, & y_6 = 1. \end{cases} \tag{A.3}$$

On the other hand, the equation (A.1) gives

$$F_n = \Psi_0 F_{n-1} + \Psi_2 F_{n-3}, \qquad n \geq 3. \tag{A.4}$$

Substituting the equation (A.2) into (A.4) and comparing the coefficients we obtain:

$$\begin{cases} x_n = x_{n-1} + 1, \\ y_n = y_{n-1} + x_{n-3}. \end{cases} \tag{A.5}$$

Solving the system (A.5) with the initial conditions (A.3) we finally obtain the propagator F_n for $n \geq 6$:

$$F_n = \Psi_0^n + (n-2)\Psi_0^{n-3}\Psi_2 + \frac{1}{2}(n-5)(n-4)\Psi_0^{n-4}\Psi_2^2, \tag{A.6}$$

which may be compared to (60).

References

[1] A.J. Lichtenberg and M.A. Lieberman, *Regular and Chaotic Dynamics* (Springer, New York, 1992).

[2] L.E. Reichl, *The Transition to Chaos in Conservative Classical Systems: Quantum Manifestations* (Springer, New York, 1992).

[3] P. Gaspard, *Chaos, Scattering and Statistical Mechanics* (Cambridge University Press, Cambridge, England, 1998).

[4] B.V. Chirikov, Phys. Rep. **52**, 265 (1979).

[5] A.B. Rechester and R.B. White, Phys. Rev. Lett. **44**, 1586 (1980); A.B. Rechester, M.N. Rosenbluth and R.B. White, Phys. Rev. A **23**, 2664 (1981).

[6] H.D.I. Abarbanel, Physica 4D, **89** (1981).

[7] J.R. Cary, J.D. Meiss, and A. Bhattacharjee, Phys. Rev. A **23**, 2744 (1981); J.R. Cary and J.D. Meiss, Phys. Rev. A **24**, 2664 (1981); J.D. Meiss, J.R. Cary, C. Grebogi, J.D. Crawford, A.N. Kaufman, and H.D.I. Abarbanel, Physica D **6**, 375 (1983).

[8] R.S. Mackay, J.D. Meiss, and I.C. Percival, Phys. Rev. Lett. **52**, 697 (1984).

[9] T. Hatori, T. Kamimura and Y.H. Hichikawa, Physica D **14**, 193 (1985).

[10] R. Artuso, E. Aurell, and P. Cvitanovic, Nonlinearity **3**, 325 (1990); *ibid.* 361 (1990).

[11] I. Dana, N.W. Murray, and I.C. Percival, Phys. Rev. Lett. **62**, 233 (1990); I. Dana , Phys. Rev. Lett. **64**, 2339 (1990); Q. Chen, I. Dana, J.D. Meiss, N.W. Murray, and I.C. Percival, Physica D **46**, 217 (1990).

[12] P. Gaspard and J. R. Dorfman, Phys. Rev. E **52**, 3525 (1995); R. Klages and J.R. Dorfman, Phys. Rev. Lett. **74**, 387 (1995); Phys. Rev. E **55**, R1247 (1997); Phys. Rev. E **59**, 5361 (1999); N. Korabel and R. Klages, Phys. Rev. Lett. **89**, 214102 (2002).

[13] M. Pollicott, Invent. Math. **81**, 413 (1985); Invent. Math. **85**, 147 (1986).

[14] D. Ruelle, Phys. Rev. Lett. **56**, 405 (1986); J. Stat. Phys. **44**, 281 (1986).

[15] H.H. Hasegawa and W.C. Saphir, Phys. Rev. A **46**, 7401 (1992).

[16] M. Khodas and S. Fishman, Phys. Rev. Lett. **84**, 2837 (2000); M. Khodas, S. Fishman and O. Agam, Phys. Rev. E **62**, 4769 (2000).

[17] R. Venegeroles, Phys. Rev. Lett. **99**, 014101 (2007); R. Venegeroles, *Leading Pollicott-Ruelle Resonances for Chaotic Area-Preserving Maps*, arXiv:0710.4779, to be published.

[18] J.A. McLennan, *Introduction to non equilibrium statistical mechanics* (Prentice Hall, Engewood cliffs, New Jersey, 1989).

[19] H. van Beijeren, Rev. Mod. Phys. **54**, 195 (1982).

[20] R. Balescu, *Statistical Dynamics, Matter out of Equilibrium* (Imperial College Press, London, 1997).

[21] G.M. Zaslavsky, Phys. Rep. **371**, 461 (2002).

[22] H.H. Hasegawa and W.C. Saphir in *Aspects of Nonlinear Dynamics: Solitons and Chaos*, edited by I. Antoniou and F. Lambert, (Springer, Berlin, 1991).

[23] M. Abramowitz and I.A. Stegun, *Handbook of Mathematical Functions* (Dover, New York, 1972).

[24] R. Tabet, D. Saifaoui, A. Dezairi, and A. Raouak, Eur. Phys. J.: Appl. Phys. **4**, 329 (1998).

[25] R. Balescu, J. Stat. Phys. **98**, 1169 (2000).

[26] O.F. Bandtlow and P.V. Coveney, J. Phys. A: Math. Gen. **27**, 7939 (1994).